

Machine learning density functional theory for the Hubbard model

James Nelson,^{*} Rajarshi Tiwari,[†] and Stefano Sanvito[‡]

School of Physics, AMBER and CRANN Institute, Trinity College, Dublin 2, Ireland

(Dated: October 31, 2018)

The solution of complex many-body lattice models can often be found by defining an energy functional of the relevant density of the problem. For instance, in the case of the Hubbard model the spin-resolved site occupation is enough to describe the system total energy. Similarly to standard density functional theory, however, the exact functional is unknown and suitable approximations need to be formulated. By using a deep-learning neural network trained on exact-diagonalization results we demonstrate that one can construct an exact functional for the Hubbard model. In particular, we show that the neural network returns a ground-state energy numerically indistinguishable from that obtained by exact diagonalization and, most importantly, that the functional satisfies the two Hohenberg-Kohn theorems: for a given ground-state density it yields the external potential and it is fully variational in the site occupation.

Density functional theory (DFT)¹ is today the most widely used method for computing the electronic structure of solids and molecules and it finds widespread applications in physics, chemistry, biology and materials science. The success of DFT has to be attributed to its solid theoretical foundation, contained in the Hohenberg-Kohn theorems², in a clear pathway to a practical implementation, formulated in the Kohn-Sham equations³, and to the possibility of constructing a hierarchical ladder of approximations for the energy functional⁴. Although DFT has been developed to solve the problem of N electrons and M nuclei interacting through the long-range Coulomb potential, one can formulate DFT-type approaches also for many-body lattice models⁵. In this case the electron density is replaced by an appropriate density defined on the lattice, which becomes the fundamental quantity of the theory. For instance, the local on-site occupation, $\{n_{i\sigma}\}$, is the relevant density of the Hubbard model. This is the expectation value of the number operator, $\hat{n}_{i\sigma} = c_{i\sigma}^\dagger c_{i\sigma}$, with $c_{i\sigma}^\dagger$ ($c_{i\sigma}$) being the fermionic creation (annihilation) operator at site i for spin $\sigma = \uparrow, \downarrow$. In the lattice DFT framework the equivalents of the two Hohenberg-Kohn theorems can be demonstrated.

The interest in lattice DFT is twofold. On the one hand, it provides a scalable numerical platform to investigate strongly correlated inhomogeneous systems as they approach the thermodynamic limit^{6,7}. On the other hand, it allows one to explore fundamental questions common to any density functional theory, such as the choice of the reference system in the construction of the energy functional⁸, the origin of the Mott gap⁹, the effects of strong correlation in quantum transport^{10–12}, the extension to the time domain^{13–15}. For some lattice models exact solutions exist. These typically concern the homogeneous case¹⁶, but they do not generalise to the inhomogeneous one¹⁷. Importantly, lattice DFT offers the ideal theoretical framework to treat on the same footing both the homogeneous and inhomogeneous problem, as we are now going to explain.

Let us consider, as an example, the standard one-dimensional Hubbard model. The Hamiltonian operator

writes

$$\hat{H}_U = \hat{T} + \hat{U} + \sum_{i\sigma} \hat{n}_{i\sigma} v_i, \quad (1)$$

where $\hat{T} = -t \sum_{i\sigma} (\hat{c}_{i+1,\sigma}^\dagger \hat{c}_{i\sigma} + \hat{c}_{i\sigma}^\dagger \hat{c}_{i+1,\sigma})$ is the kinetic energy with hopping parameter t , $\hat{U} = U \sum_{i=1} \hat{n}_{i\uparrow} \hat{n}_{i\downarrow}$ is the Coulomb repulsion of strength $U > 0$, and the last term describes the interaction with an external potential $\{v_i\}$. If $v_i = v_0$ for every site i , one has the homogeneous case. The first Hohenberg-Kohn theorem establishes the existence of an energy functional,

$$E[\{n_{i\sigma}\}] = F[\{n_{i\sigma}\}] + \sum_{i\sigma} n_{i\sigma} v_i, \quad (2)$$

$$F[\{n_{i\sigma}\}] = \langle \Psi | \hat{T} + \hat{U} | \Psi \rangle, \quad (3)$$

where $F[\{n_{i\sigma}\}]$ is universal and independent from the external potential, v_i . This means that there is a one-to-one correspondence between the density and the external potential, namely the knowledge of the former is enough to uniquely determine the latter. Since the functional is universal, lattice DFT can be applied identically to both the homogeneous and the inhomogeneous problem. Note that for this lattice model $F[\{n_{i\sigma}\}]$ is universal only for a given \hat{T} and \hat{U} operator. This has some important consequences. For instance, even in one dimension, arranging the sites in a ring or in a chain geometry yields two different \hat{T} 's. This means that $F[\{n_{i\sigma}\}]$ for a ring is different from $F[\{n_{i\sigma}\}]$ for a chain, even if both t and U remain the same. Finally the second Hohenberg-Kohn theorem guarantees that the energy functional is minimised at the ground-state density, $\{n_{i\sigma}^{\text{GS}}\}$, to yield the ground-state energy, E^{GS} , namely $E[\{n_{i\sigma}\}] \geq E[\{n_{i\sigma}^{\text{GS}}\}] = E^{\text{GS}}$.

As for standard DFT even in the lattice case the exact functional is not known and approximations need to be formulated. These vary depending on the specific problem and usually proceed by interpolation from known exact solutions. Here we take a completely different approach and we construct an *exact* functional by using a machine learning model trained on exact diagonalization results. Machine learning (ML) models form a large

class of algorithms, which have been traditionally used for data processing and analysis. Recently these numerical techniques have found a common place in many-body problems¹⁸, phase transitions^{19–21}, Green’s functions calculation²², and in the solution of single-particle problems in an arbitrary potential²³.

“Supervised” ML algorithms construct a one-to-one correspondence between vectors or between vectors and scalars. We can then formulate the search for the energy functional as a ML problem, namely we can search for a non-analytic function, f_{ML} , which associates to a given density (the vector of site occupation $\{n_{i\sigma}\}$) the corresponding energy. In particular our strategy consists in solving exactly the many-body problem for a set of different randomly chosen external potentials, $\{v_i\}$, and then to use the calculated ground-state density and ground-state energy to define the ML model. In practice we compute

$$f_{\text{ML}} : \{n_{i\sigma}^{\text{GS}}\} \rightarrow E^{\text{GS}} - \sum_{i\sigma} n_{i\sigma}^{\text{GS}} v_i = \langle \Psi^{\text{GS}} | \hat{T} + \hat{U} | \Psi^{\text{GS}} \rangle, \quad (4)$$

where $|\Psi^{\text{GS}}\rangle$ is the many-body ground-state wave function. The fact that we use a set of random external potentials effectively allows us to explore a broad range of densities, and hence to map accurately the functional.

We apply our strategy to the one-dimensional Hubbard model for a system of $L = 8$ sites arranged in a ring geometry (periodic boundary conditions). Furthermore we restrict ourself to the paramagnetic quarter filling case, where the total number of electrons is $N = 4$ and we have $N_{\uparrow} = N_{\downarrow} = 2$. In order to fully determine the model we set²⁴ $U = 4$ and $t = 1$ and, as mention before, we construct the dataset for the ML model by exact diagonalization²⁵. The random external potential is taken according to a uniform distribution with $v_i \in [-W, +W]$. In particular we have constructed several external potential distributions with W varying between $0.005t$ and $2.5t$. Furthermore, in order to prevent the dataset from having large fluctuations in the total energy we neglect potentials yielding to total energies $0.15t$ larger than that of the homogeneous case. Note that the $SU(2)$ symmetry of the problem and the condition $N_{\uparrow} = N_{\downarrow}$ also guarantee that the local site occupation remains spin unpolarised, namely we have $n_{i\uparrow} = n_{i\downarrow}$. This means that in the special case investigated here the functional depends only on one of the two spin densities, for instance on $\{n_{i\uparrow}\}$.

In order to increase the size of the dataset without performing further exact diagonalization steps we include configurations obtained from the calculated ones by applying the allowed symmetry operations. In particular for any potential v_i the mirror-symmetric potential $v_i \rightarrow v_{L+1-i}$ yields a mirror-symmetric charge density with identical total energy. A similar situation applies to potentials obtained by translation, namely $v_i \rightarrow v_{i+1}$. Examples of the charge density profiles obtained with such symmetry operations are presented in the inset of Fig. 1. The addition of such configurations drastically improves the ML model. The improvements has two

main origins. On the one hand the dataset is larger. On the other hand the inclusion of the degenerate configurations allows the model to learn about the symmetries of the system.

In the construction of the ML model the dataset is split into four mutually exclusive subsets. The training set, containing 52,500 samples, is used to train the model. The validation set, containing 26250 samples, is employed to select the best ML model. The test set, also containing 26250 samples, serves to estimate the generalization error of the model, namely how well it performs on new data never seen before. Finally we set aside 100 configurations to test the gradient descent scheme for the demonstration of the second Hohenberg-Kohn theorem. These latter configurations are chosen uniformly over energy such that the entire range is explored. The structure of our dataset is presented in Fig. 1. In the figure we plot the ground-state total energy as a function of the euclidean distance of the corresponding charge density with respect to that of the homogeneous case, $n_{i\sigma} = 1/4$. Larger euclidean distances are associated to the choices of external potential with larger fluctuations. As expected, the distribution of total energies gets broader as the deviation from the homogenous case gets larger. Note that the homogeneous case, $v_i = 0$, is associated to the minimum of the distribution, where we have $E^{\text{GS}} = F[\{1/4\}]$.

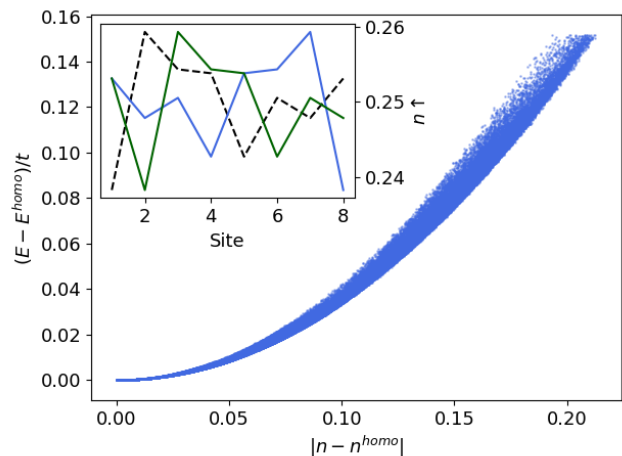


FIG. 1. (Color online) Structure of the data used to construct the ML model. We plot the ground-state total energy as a function of the euclidean distance of the corresponding charge density with respect to that of the homogeneous case, $n_{i\sigma} = 1/4$, for a large selection of external potentials, $\{v_i\}$. The total energy is measured with respect of that of the $v_i = 0$ case, which corresponds to $E^{\text{homo}} = F[\{1/4\}]$. Note that the data points in the main plot are those generated numerically and do not consider the symmetries of the system. In the insert we show examples of charge densities constructed from a given one (dashed line) by applying the symmetry operations of the system: mirror symmetry (blue line) and the translational symmetry (green line).

After having tested a few ML models we have opted for a convolutional neural network, which is found to perform better than standard neural networks²⁶. All the machine learning algorithms have been implemented by using the Keras python package²⁷. In the convolutional neural network in order to fully capture all the information we extend each of the occupation vectors, by adding their first k components on to the end of the vector, thus creating a $L + k$ component-long vector. In doing so k is the size of the one-dimensional convolution window, in our particular case $k = 3$. This procedure allows us to encode the interaction between the sites at the end and the sites at the beginning of the vector. The convolution neural network used has 8 convolutional filters, followed by 2 fully connected layers each with 128 units and finally an output layer.

The accuracy of our ML model can be appreciated by looking at the upper panel of Fig. 2, where we present the residual of the predicted $F[\{n_{i\sigma}^{\text{GS}}\}]$, namely $F_{\text{exact}}^{\text{GS}} - f_{\text{ML}}$, calculated over the test set against the predicted results. From the figure it can be clearly appreciated that the ML model is almost indistinguishable from the exact functional. Its mean error over the entire test set is in fact $0.0002t$, namely it is of the order of 0.02%. This remarkable accuracy confirms that the functional has been fully learned by our ML model.

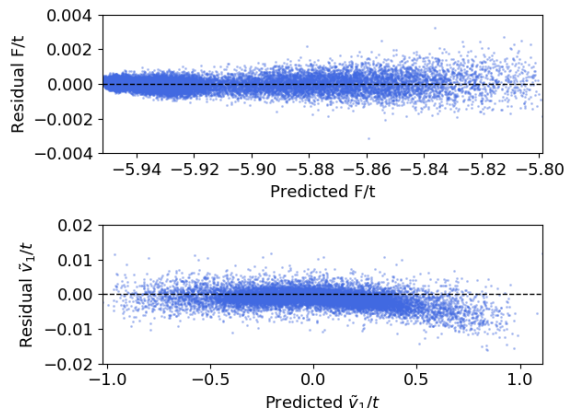


FIG. 2. Numerical accuracy of the ML model measured by the residuals, namely the difference between a predicted quantity and its exact value. In the upper panel we show the residual of f_{ML} as a function of the corresponding exact-diagonalization result for the entire test set. The model is almost indistinguishable from the exact results, demonstrating that f_{ML} is the exact functional. The mean absolute error is $0.0002t$, namely it is about 0.02%. In the lower panel we present a numerical demonstration of the first Hohenberg-Kohn theorem. The residual of the external potential at site $i = 2$, measured with respect to that at site $i = 1$, $\tilde{v}_1 = v_2 - v_1$, is plotted against the exact value for the entire test set. The mean absolute error is $0.001t$. Similar curves can be obtained for the other on-site energies.

We now proceed to demonstrate that the ML functional, f_{ML} , satisfies both the Hohenberg-Kohn theo-

rems. The first Hohenberg-Kohn theorem states that the ground state density uniquely determines the external potential up to a constant². In order to numerically demonstrate the theorem we take the convolutional neural network constructed before and we generate as an output a seven-component vector. This contains the external potential, namely the on-site energies $\{v_i\}$, which are measured by imposing that the potential of the first site is $v_1 = 0$. Such constrain ensures that that all the potentials are determined with the same constant. In other words our constant-rescaled external potential is the vector

$$\tilde{\mathbf{v}} = (v_2 - v_1, v_3 - v_1, \dots, v_L - v_1). \quad (5)$$

The numerical proof of the first Hohenberg-Kohn theorem is presented in the lower panel of Fig. 2, where we compare the residual of the first component of $\tilde{\mathbf{v}}$, namely $\tilde{v}_1 = v_2 - v_1$, against the exact results. As before the agreement over the entire test set is nearly perfect with a mean absolute error of $0.001t$. Similar agreements are found for the other on-site energies, so that one has to conclude that $0.001t$ is the precision of our ML model to determine the external potential.

Finally we proceed to demonstrate the second Hohenberg-Kohn theorem, namely we show that the ground-state energy can be found as the minimum of the universal functional at the ground-state density. Strictly speaking this information was not explicitly used in the construction of our ML functional, since f_{ML} interpolates only at the ground state and not around it. However, since our data set includes a vast number of external potentials, it includes a vast number of different densities. As such f_{ML} has been *de facto* constructed by extensively exploring the entire density landscape. The minimization of the energy functional (2) is carried out by gradient descent²⁶. The generic derivative of $E[\{n_{i\sigma}\}]$ writes

$$\frac{\partial E}{\partial n_{j\sigma'}} = v_j + \frac{\partial}{\partial n_{j\sigma'}} F[\{n_{i\sigma}\}], \quad (6)$$

where the gradient of the ML model, $F[\{n_{i\sigma}\}] = f_{\text{ML}}$, is estimated by using second order finite-differences. The search for the minimum must also satisfy two conditions, namely $0 \leq n_{i\sigma} \leq 1$ and particle conservation, $\sum_{i=1}^L n_{i\sigma} = N_{\sigma}$. The first condition is imposed by simply halting the gradient descent algorithm, whenever it is violated. In contrast the second one is enforced by normalizing the occupations after each update.

The accuracy of the computed site occupations is measured as

$$\delta n = \sqrt{\sum_{i\sigma} |n_{i\sigma} - n_{i\sigma}^{\text{exact}}|^2} = \sqrt{2} \sqrt{\sum_i |n_{i\uparrow} - n_{i\uparrow}^{\text{exact}}|^2}, \quad (7)$$

where $n_{i\sigma}^{\text{exact}}$ is the exact site occupation and the second equality follows from $n_{i\uparrow} = n_{i\downarrow}$. Similarly we compute the difference in energy from the reference system. In particular we perform two tests. In the first one we set

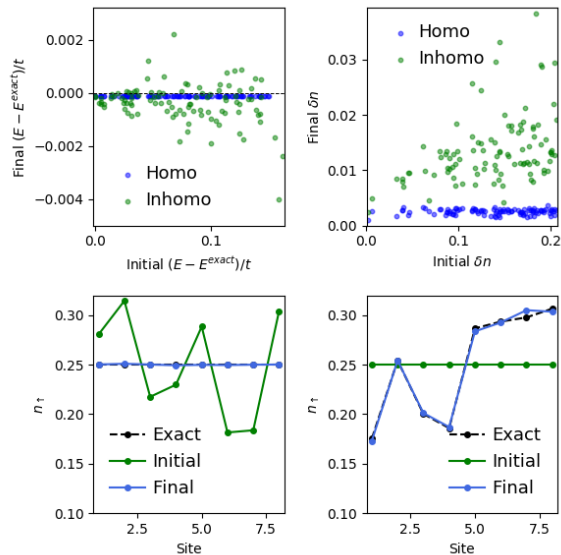


FIG. 3. Numerical demonstration of the second Hohenberg-Kohn theorem. The top two panels show the error in the final converged energy (left) and density (right) [see Eq. (7)] as a function of the distance of the initial quantity from the exact one. Note that when searching for the homogeneous density/energy (blue dots) the gradient descent algorithm appears more accurate than when looking for the inhomogeneous one (green dots). The two lower panels show examples of the converged occupations, when searching for the ground state density of either the homogeneous (left) or the inhomogeneous (right) system.

the external potential to $v_i = 0$ and search for $\{n_{i\sigma}\}$ and $F[\{n_{i\sigma}\}]$ corresponding to the homogeneous case starting from a random non-homogeneous occupation. In the second one we start from the homogeneous occupation and test the convergence to $\{n_{i\sigma}^{\text{GS}}\}$ corresponding to the inhomogeneous potential $v_i \neq 0$. Such exercise is performed over the gradient descent set (100 samples) and the results are presented in Fig. 3.

The two top panels demonstrate that f_{ML} is variational. In these we show the difference in the energy (left-hand side panel) and site occupation (right-hand side panel) between the expected exact values and that found by gradient descent, with respect to their initial value. This effectively explores how well f_{ML} has learned about the energy functional landscape, and looks at how

close it converges to the ground-state energy and occupation as a function of how far the initial occupation/energy was. We use blue dots when searching for the ground state of the homogeneous case and green ones for that of the inhomogeneous. If f_{ML} is exact all dots will be on an horizontal straight line at zero. In general we find that the ground-state quantities (energy and density) are reached within a few percent regardless of their initial value. When searching for the ground state of the homogeneous system the error is minimal and almost independent from the initial condition. In contrast the search for $\{n_{i\sigma}^{\text{GS}}\}$ and E^{GS} corresponding to an inhomogeneous potential is less accurate and the average error grows linearly with the distance from the initial occupation from the final one.

The two lower panels instead display two examples of converged site occupation. The left-hand side panel show that one can recover the homogeneous occupation when the gradient descent starts from an inhomogeneous one, while that on the right-hand side depicts the opposite, namely that an almost exact inhomogeneous occupation can be found by starting from the homogeneous one.

In conclusion we have used machine learning to construct the exact energy functional for the inhomogeneous Hubbard model. This is provided by a convolutional neural network constructed over exact results obtained by exact diagonalization. The functional appears numerically indistinguishable from the exact solutions and satisfies both the Hohenberg-Kohn theorems, namely it establishes a one-to-one correspondence between the site occupation and the external potential, and it is variational. Here the functional was constructed for the quarter filling diamagnetic case, but the same procedure can be applied to any filling factors and number of sites, including the possibility to describe magnetic ground states. Our results demonstrate that ML can be used to define exact density functional theories and offer the potential to be expanded to other lattice and continuous models.

Acknowledgments

Funding is provided by the Irish Research Council (JN) and by the European Research Council project QUEST (RT). We acknowledge the DJEI/DES/SFI/HEA Irish Centre for High-End Computing (ICHEC) and Trinity Centre for High Performance Computing (TCHPC) for the provision of computational resources.

* janelson@tcd.ie

† tiwarir@tcd.ie

‡ stefano.sanvito@tcd.ie

¹ W. Kohn, Rev. Mod. Phys. **71**, 1253 (1999).

² P. Hohenberg and W. Kohn, Phys. Rev. **136** B864, (1964).

³ W. Kohn and L.J. Sham, Phys. Rev. **140**, A1133 (1965).

⁴ J.P. Perdew, A. Ruzsinszky, J. Tao, V.N. Staroverov, G.E. Scuseria and G.I. Csonka, J. Chem. Phys. **123**, 062201 (2005).

⁵ K. Schönhammer, O. Gunnarsson and R.M. Noack, Phys. Rev. B **52**, 2504 (1995).

⁶ F.C. Alcaraz and K. Capelle, Phys. Rev. B **76**, 035109 (2007).

- ⁷ M. Saubané and G.M. Pastor, Phys. Rev. B **84**, 035111 (2011).
- ⁸ N.A. Lima, M.F. Silva, L.N. Oliveira and K. Capelle, Phys. Rev. Lett. **90**, 146402 (2003).
- ⁹ N.A. Lima, L.N. Oliveira and K. Capelle, Eur. Phys. Lett. **60**, 601 (2002).
- ¹⁰ G. Stefanucci and S. Kurth, Phys. Rev. Lett. **107**, 216401 (2011).
- ¹¹ V. Vettchinkina, A. Kartsev, D. Karlsson and C. Verdozzi, Phys. Rev. B **87**, 115117 (2013).
- ¹² A. Pertsova, M. Stamenova and S. Sanvito, J. Phys.: Condens. Matter **25**, 105501 (2013).
- ¹³ C. Verdozzi, Phys. Rev. Lett. **101**, 166401 (2008).
- ¹⁴ D. Karlsson, A. Privitera and C. Verdozzi, Phys. Rev. Lett. **106**, 116401 (2011).
- ¹⁵ A. Akande and S. Sanvito, J. Phys.: Condens. Matter **24**, 055602 (2012).
- ¹⁶ E.H. Lieb and F.Y. Wu, Phys. Rev. Lett. **20**, 1445 (1968).
- ¹⁷ F.H.L. Essler, H. Frahm, F. Göhmann, A. Klümper and V.E. Korepin, *The One-Dimensional Hubbard Model*, Cambridge University Press (2009).
- ¹⁸ G. Carleo and M. Troyer, Science **355**, 602 (2017).
- ¹⁹ J. Carrasquilla and R.G. Melko, Nature Phys. **13**, 431 (2017).
- ²⁰ K. Ch'ng, J. Carrasquilla, R.G. Melko and E. Khatami, Phys. Rev. X **7**, 031038 (2017).
- ²¹ P. Broecker, J. Carrasquilla, R.G. Melko, and Simon Trebst, Scientific Reports **7**, 8823 (2017).
- ²² L.-F. Arsenault, A. Lopez-Bezanilla, O.A. von Lilienfeld and A.J. Millis, Phys. Rev. B **90** 155136 (2014).
- ²³ K. Mills, M. Spanner and I. Tamblin, Phys. Rev. A **96**, 042113 (2017).
- ²⁴ Throughput the paper we measure all energies in unit of t .
- ²⁵ M. Sharma and M.A.H. Ahsan, Comp. Phys. Comm. **193**, 19 (2015).
- ²⁶ I. Goodfellow, Y. Bengio and A. Courville, *Deep learning*, MIT Press, Cambridge (2016). <http://www.deeplearningbook.org>
- ²⁷ F. Chollet et al., *Keras: The Python Deep Learning library*, <https://keras.io> (2015).